

Heterogeneous crystallization and composition dependence of optical parameters in Sn–Sb–Bi–Se chalcogenides

Muneer Ahmad · R. Thangaraj · T. Stephen Sathiaraj

Received: 5 November 2008 / Accepted: 22 November 2009 / Published online: 10 December 2009
© Springer Science+Business Media, LLC 2009

Abstract Bulk samples of $\text{Sn}_{10}\text{Sb}_{20-x}\text{Bi}_x\text{Se}_{70}$ ($0 \leq x \leq 8$) chalcogenide alloys were prepared by the conventional melt quenching technique. Thin films were prepared on well-cleaned glass substrates by thermal evaporation technique. X-ray diffraction studies revealed that the alloys with $x = 0$ and 2 at.% of Bi were amorphous, whereas the alloys with $x = 4, 6, 8$ at.% were crystalline. The crystalline phases are identified as due to the formation of Bi_2Se_3 and BiSe_2 phases. The microstructural and differential scanning calorimetric studies show the presence of these phases. A simple, straight forward procedure suggested by Swanepoel has been used to calculate the optical parameters, refractive index, and extinction coefficient. The optical gap for all the samples has been obtained from the Tauc plots. The variation in optical parameters for different Bi concentration has been explained on the basis of presence of defect states and the change in stoichiometry with the change in Bi concentration.

Introduction

Chalcogenide glasses have attracted considerable interest due to their infrared transparency, low phonon energies, and high non-linear optical parameters [1–4]. They are promising materials for grating and switching devices, and optical memories [5–7]. Recently, these glasses have been

used as core materials for high-efficiency fiber amplifiers due to their high refractive indices and very low phonon energy [8, 9]. Understanding the nature of the microscopic structure of glassy materials and the relationship between the structure and the observed macroscopic material properties have been the challenging problems in condensed matter physics. In particular, much attention has been devoted to understanding the characteristics of the structural network of chalcogenide glasses, important as IR optical materials [10–12]. A number of concepts have been developed to understand the network disorder of these glassy solids and its influence on their mechanical, thermal, and optical properties. The study of Sn–Sb–Se glasses has been of recent interest due to their small glass-forming region [13] as compared to other alloys from the IV–V–VI ternary system, where light mass elements were used. The incorporation of Bi in Sn–Sb–Se ternary alloy system, like many other chalcogenide systems, is expected to show good optical and electrical behaviors. As reported by various researchers, the incorporation of a critical amount of Bi leads to carrier-type reversal that is a change over from *p*- to *n*-type in these materials [14–16]. A proper description of the structural, optical, and electrical properties of Sn–Sb–Bi–Se system is important for a fundamental understanding of their properties and applications. The optical band gap and refractive index are the most significant parameters in amorphous semiconducting thin films. For example, the change in the refractive index between the amorphous and the crystalline states in the visible wavelength is very important for phase change recording. In this study, we examined the structural profile and optical constants of the Sn–Sb–Bi–Se system. This article reports the structural changes with the help of X-ray diffractometry, scanning electron microscopy, and thermal studies with the addition of Bi. It also reports the change in optical

M. Ahmad · R. Thangaraj (✉)
Semiconductors Laboratory, Department of Applied Physics,
Guru Nanak Dev University, Amritsar, Punjab 143005, India
e-mail: rthangaraj@rediffmail.com

T. S. Sathiaraj
Department of Physics, University of Botswana, Gaborone,
Botswana

parameters such as optical gap, refractive index, and so on, with the addition of Bi.

Experimental

Five different compositions of $\text{Sn}_{10}\text{Sb}_{20-x}\text{Bi}_x\text{Se}_{70}$ ($0 \leq x \leq 8$) alloys were prepared by the conventional melt quenching technique. Granules of Sn, Sb, Bi, and Se having 99.999% purity were used to prepare the samples. These samples were batched in a closed-scale balance on which Sn, Sb, Bi, and Se were weighed according to their atomic percentage and were sealed in a quartz ampoule (10-mm long and 6 mm internal diameter), in a vacuum better than 10^{-4} mbar. The sealed ampoule was kept in a vertical furnace where the temperature was raised to 1123 K at a rate of 4–5 K/min. The ampoule was inverted at a regular interval (~ 1 h) for 48 h at the maximum temperature to insure the homogeneous mixing of the constituents, before quenching in an ice bath. The material was separated from the quartz ampoule by dissolving the tube into a solution of $\text{HF} + \text{H}_2\text{O}_2$ for approximately 48 h. Differential scanning calorimetric (DSC) runs were carried out using Mettler Toledo Star[®] instrument under non-isothermal conditions. The DSC was calibrated with standard materials prior to start of the experiment. All the DSC scans were performed under N_2 atmosphere. About 25 mg of the powdered sample was placed in the aluminum pans for studies. A PHILIPS X-ray diffractometer (PW3710 mpd with a PW1830 generator) was used to identify the amorphous/crystalline phases in the prepared bulk samples. The film deposition was carried out in a high vacuum system (HINDHI VAC coating unit, Model No. 12A4D) in a pressure of 10^{-5} mbar. The film deposition was carried out on well-cleaned glass slides kept at room temperature as substrates and with source material taken in a molybdenum boat. The surface morphology was studied with scanning electron microscope (SEM) (PHILIPS XL 30 ESEM system). The optical transmission and reflection spectrum were recorded at room temperature for all the samples using UV-Vis spectrophotometer (VARIAN Cary500 UV-VIS-NIR) in the wavelength range 400–2500 nm.

Results and discussion

Structural analysis

Figures 1 and 2 show the X-ray diffractograms for the as-prepared powder samples of $\text{Sn}_{10}\text{Sb}_{20-x}\text{Bi}_x\text{Se}_{70}$ ($0 \leq x \leq 8$) alloys. Figure 1 shows that the compositions with $x = 0$ and 2 at.% of Bi are typical glasses without any sharp peak in the diffractograms, whereas the diffractograms of

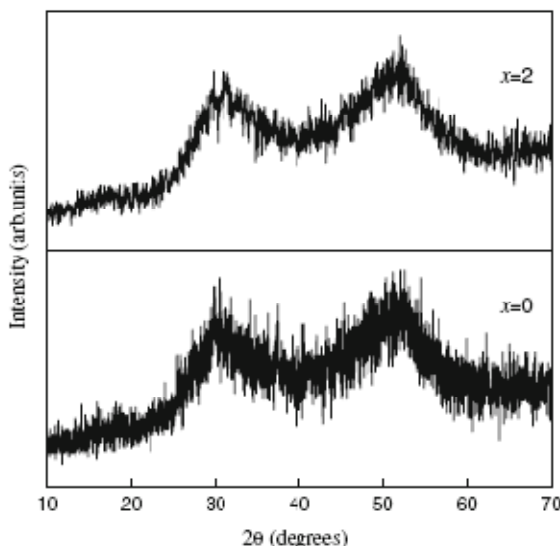


Fig. 1 The X-ray diffraction patterns for the as-prepared $\text{Sn}_{10}\text{Sb}_{20-x}\text{Bi}_x\text{Se}_{70}$ ($x = 0$ and 2) powder samples

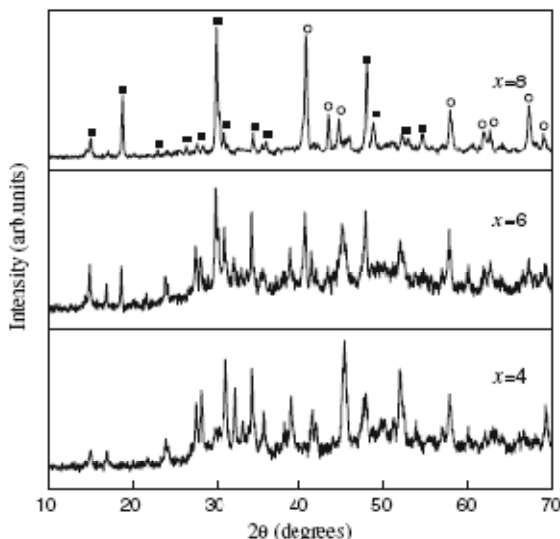


Fig. 2 X-ray diffractograms for the as-prepared $\text{Sn}_{10}\text{Sb}_{20-x}\text{Bi}_x\text{Se}_{70}$ ($x = 4, 6, 8$) powder samples

samples with $x = 4, 6,$ and 8 at.% show strong peaks which indicate the existence of microcrystallites in these samples as observed from Fig. 2. Different peaks were identified using the JCPDS database (1997). These crystalline peaks are due to the formation of Bi_2Se_3 (circle) and BiSe_2 (filled square) phases. This indicates that the alloy consists of small grains of the Bi_2Se_3 and BiSe_2 (at lower Bi concentration $x = 4$) phases as supported by the SEM studies discussed

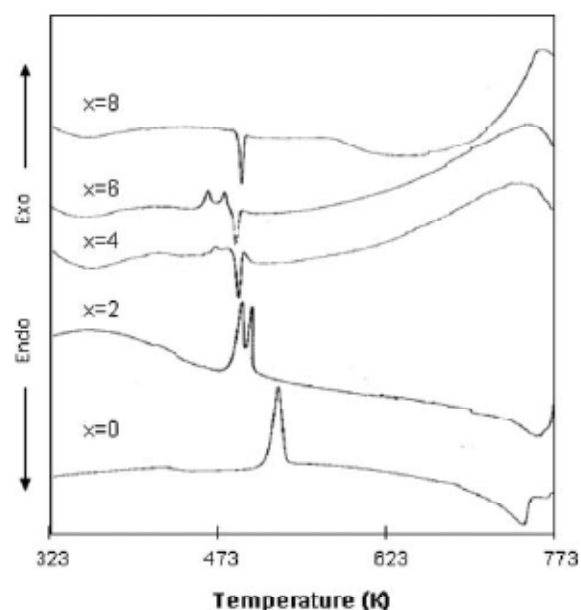


Fig. 3 DSC thermograms for the $\text{Sn}_{10}\text{Sb}_{20-x}\text{Bi}_x\text{Se}_{70}$ ($x = 0, 2, 4, 6, 8$) samples at a heating rate of 10 K/min

later and the size of these grains increase with further addition of Bi content. DSC thermograms obtained at a heating rate of 10 K/min for the $\text{Sn}_{10}\text{Sb}_{20-x}\text{Bi}_x\text{Se}_{70}$ ($x = 0, 2, 4, 6, 8$) system are shown in Fig. 3. All the thermograms show glass transition, crystallization, and melting temperatures. Two exothermic peaks due to crystallization were observed for all the compositions except for the $\text{Sn}_{10}\text{Sb}_{12}\text{Bi}_8\text{Se}_{70}$ (i.e., for $x = 8$) system as shown in Fig. 3. The presence of two peaks means that there are two phases appearing during the crystallization process. The phases in which the alloy crystallizes after the thermal process may be the same phases observed in X-ray diffractograms for $x = 4, 6, 8$ as discussed earlier. Figure 3 shows that T_g shifts toward higher temperature with increase in Bi concentration. Samples with all x values show similar behavior. In the system under study, the glass transition temperature is found to increase with the increase in heating rate as well as with the addition of Bi content. The increase in the value of T_g with bismuth content can be explained with the help of chemically ordered network model according to which the heteropolar bond is favored over the homopolar bond [17]. The heteronuclear bond energies U_{A-B} between unlike atoms A and B are calculated using homonuclear bond energies, namely U_{A-A} and U_{B-B} , and the difference in electro-negativities of the two atoms ($X_A - X_B$):

$$U_{A-B} = 0.5[U_{A-A} + U_{B-B}] + 23(X_A - X_B)^2 \quad (1)$$

where Pauling's electro-negativities of Sn, Sb, Bi, and Se are 1.96, 2.05, 2.02, and 2.55, respectively. The various

types of bonds expected in this system are Se–Se, Sn–Sn, Sb–Sb, Sn–Se, Sb–Se, and Sn–Sb. When Bi is introduced, it is expected to combine with Se followed by a decrease in the concentration of Sb–Se bonds because the bond energy of Bi–Se bonds (280.3 kJ/mol) is larger than the Sn–Se (267.81 kJ/mol) bonds [18, 19]. Therefore, the composition dependence of T_g is explained by the formation of Bi–Se bonds. The values of T_g are much higher than room temperature. This is an important advantage of these alloys, due to the fact that higher T_g value as compared to room temperature is essential to avoid self-transition of recording materials between the two phases; amorphous and crystalline phases at room temperature.

The surface morphology of the thermally evaporated $\text{Sn}_{10}\text{Sb}_{20-x}\text{Bi}_x\text{Se}_{70}$ system was observed using SEM. Figure 4a–c shows the images of $\text{Sn}_{10}\text{Sb}_{20-x}\text{Bi}_x\text{Se}_{70}$ ($x = 2, 4, 6$) thin films deposited on glass substrates. As observed from Fig. 4a, the surface appears smooth having featureless background which means that for $x = 2$ at.%, the system remains amorphous which is already confirmed from the X-ray diffractograms. The further addition of Bi content ($x = 4$) leads to the appearance of small-sized grains shown in Fig. 4b which are due to the formation of Bi_2Se_3 and BiSe_2 phases as identified from the X-ray diffractograms with the help of JCPDS files. For $x = 6$ at.% of Bi, these small-sized grains fused together to produce large irregular-sized grains or the clusters of Bi_2Se_3 and BiSe_2 as shown in Fig. 4c.

Optical parameters

Optical transmission (T) is a very complex function and is strongly dependent on the absorption coefficient (α). Figure 5 shows the variation of transmission (T) spectra with wavelength (λ) in $\text{Sn}_{10}\text{Sb}_{20-x}\text{Bi}_x\text{Se}_{70}$ ($0 \leq x \leq 8$) thin films, respectively. The refractive index of the thin films is obtained by the envelope method proposed by Swanepoel [20], by making use of the following expressions: in the transparent region, where the absorption coefficient $\alpha \approx 0$, the value of n is given by

$$n = \left[N + (N^2 - s^2)^{1/2} \right]^{1/2}, \quad (2)$$

where

$$N = \frac{2s}{T_m} - \frac{(s^2 + 1)}{2}, \quad (3)$$

where T_m is the envelope function of minimum transmittance and s is the refractive index of the substrate of value 1.5. In the weak region where the absorption coefficient $\alpha \neq 0$, the transmittance due to the influence of α and the value of N in Eq. 2 is given by

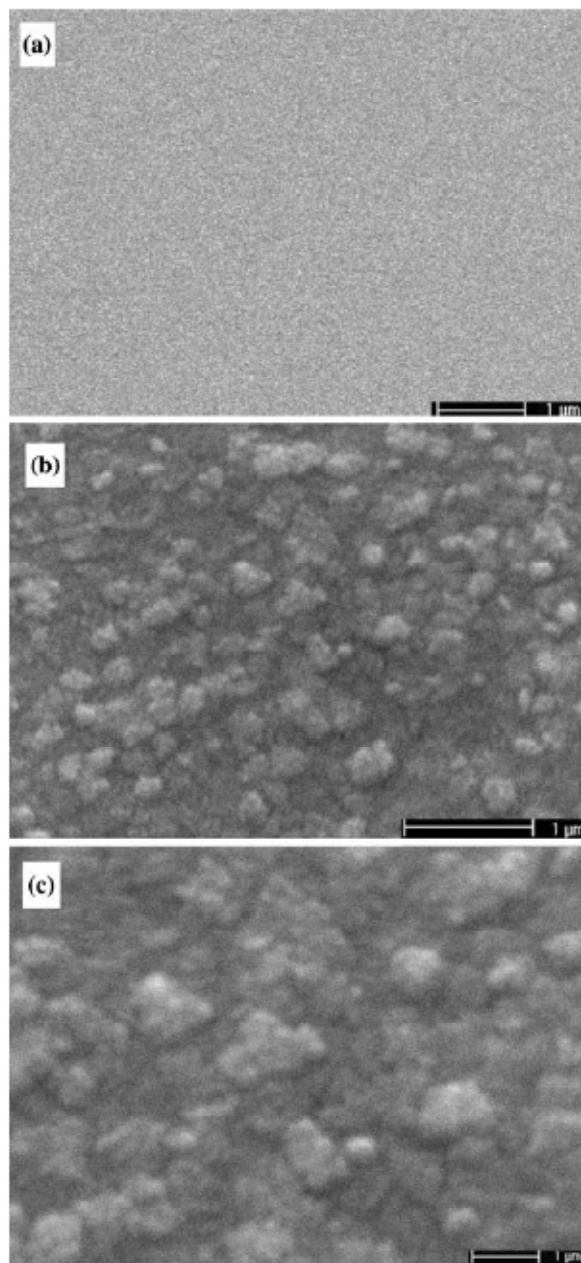


Fig. 4 a–c SEM micrographs for the $\text{Sn}_{10}\text{Sb}_{20-x}\text{Bi}_4\text{Se}_{70}$ ($x = 2, 4, 6$) thin films

$$N = 2s \frac{T_M - T_m}{T_M T_m} + \frac{(s^2 + 1)}{2}, \quad (4)$$

where T_M is the envelope function of maximum transmittance. The accuracy of the refractive index can be increased by calculating the thickness of the thin films (d), taking into account the basic interference equation

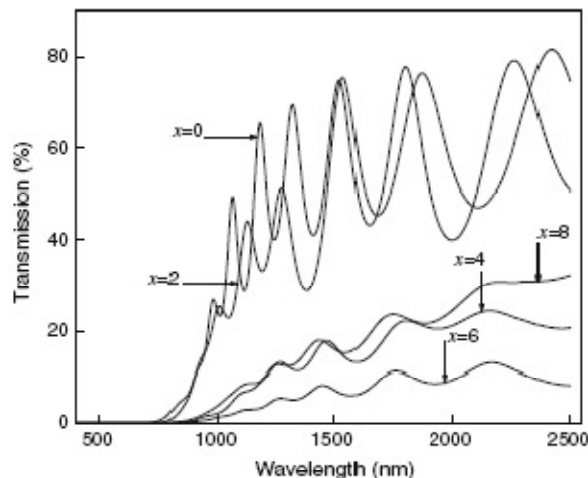


Fig. 5 Transmission spectrum of $\text{Sn}_{10}\text{Sb}_{20-x}\text{Bi}_4\text{Se}_{70}$ ($0 \leq x \leq 8$) thin films

$$2nd = m\lambda, \quad (5)$$

where $m = 1, 2, 3, \dots$ at the maximum points in the transmission spectrum and $m = 1/2, 3/2, 5/2, \dots$ at the minimum points in the transmission spectrum. If n_1 and n_2 are the refractive indices of two adjacent maxima or minima at wavelengths λ_1 and λ_2 , then the thickness of the films is given by

$$d = \frac{\lambda_1 \lambda_2}{2(\lambda_1 n_2 - \lambda_2 n_1)}. \quad (6)$$

The extinction coefficient k can be calculated using the relation

$$k = \frac{\lambda}{4\pi d} \ln\left(\frac{1}{X}\right), \quad (7)$$

where d is the thickness of the film and X is the absorbance. In the region of weak and medium absorption using the transmission maxima, X can be calculated by

$$X = \frac{E_M - [E_M^2 - (n^2 - 1)^3(n^2 - s^4)]^{0.5}}{(n - 1)^3(n - s^2)}, \quad (8)$$

where

$$E_M = \frac{8n^2s}{T_M} + (n^2 - 1)(n^2 - s^2). \quad (9)$$

The variation of the refractive index and the extinction coefficient with wavelength is shown in Fig. 6. From Fig. 6, it is clear that both the refractive index and the extinction coefficient decrease with the increase in wavelength for all compositions. The decrease in the value of refractive index with wavelength shows the normal dispersion behavior of the material. Moreover, this decrease in the extinction coefficient with an increase in wavelength

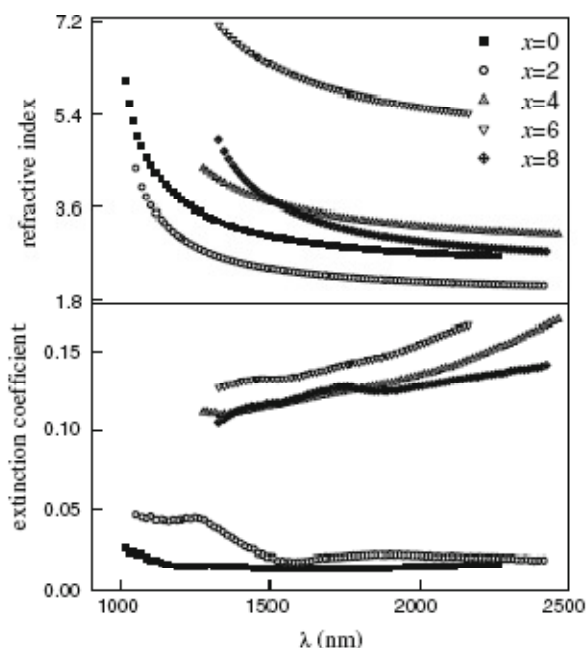


Fig. 6 Plot of refractive index and extinction coefficient versus wavelength for $\text{Sn}_{10}\text{Sb}_{20-x}\text{Bi}_x\text{Se}_{70}$ ($0 \leq x \leq 8$) thin films

Table 1 Values of refractive index (n), extinction coefficient (k) at 1500 nm, and optical gap (E_g^{opt}), band tailing parameter (B^{-1}), and thickness (d) for the $\text{Sn}_{10}\text{Sb}_{20-x}\text{Bi}_x\text{Se}_{70}$ ($0 \leq x \leq 8$) thin films

x	n	k	E_g^{opt} (eV)	B^{-1} (cm-eV)	d (nm)
0	3.07	0.01	1.19	578.57	1273
2	2.42	0.02	1.23	593.02	1079
4	3.69	0.11	1.03	440.49	1250
6	6.34	0.13	1.01	380.33	1250
8	3.73	0.11	0.99	401.90	1169

also shows that the fraction of light lost due to scattering and absorbance process decreases. The variation of both n and k with Bi concentration for all the films at 1500 nm is given in Table 1. As observed from Table 1, the change in both the optical parameters may be due to the change in stoichiometry and internal strain of the glassy alloy with the change in Bi concentration.

The absorption coefficient α was computed from the experimental measured values of R and T according to the following approximate relation

$$T = (1 - R)^2 \exp(-\alpha d) \tag{10}$$

where d is the thickness of the investigated films. The optical band gap has been estimated from the absorption coefficient data as a function of wavelength using the Tauc [21] relation

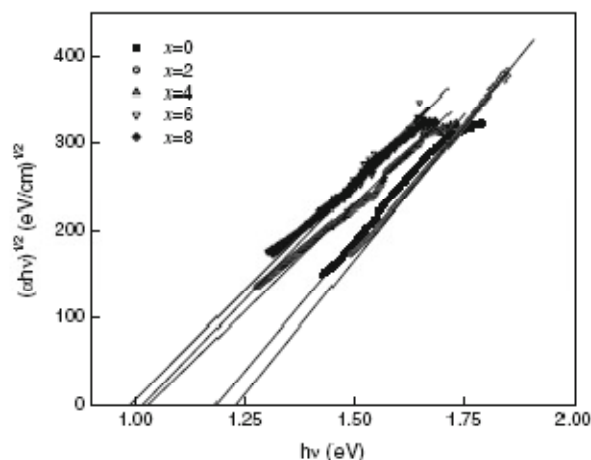


Fig. 7 Plot showing the variation of $(\alpha hv)^{1/2}$ with (hv) for the $\text{Sn}_{10}\text{Sb}_{20-x}\text{Bi}_x\text{Se}_{70}$ ($0 \leq x \leq 8$) samples

$$(\alpha hv) = B(hv - E_g)^2, \tag{11}$$

where hv is the photon energy, α is the absorption coefficient, E_g is the optical gap, B is the band tailing parameter, and $n = 1/2$ and 2 for direct and indirect band gaps, respectively.

Figure 7 shows a plot of $(\alpha hv)^{1/2}$ versus (hv) for different Bi concentrations ($0 \leq x \leq 8$) for the investigated films. The optical gap is calculated by taking the intercept on the energy axis. The variation of the optical band gap with different Bi concentrations is listed in Table 1. As observed from Table 1, the band gap initially increases for $x = 2$ Bi concentration and then decreases sharply for all the samples ($x = 4, 6, 8$). These results could be understood in terms of the modifications of the network with the increase in Bi content. The homogeneous mixing at the lower concentrations and the formation of strong Bi–Se bonds in the network, with consequent decrease in the defect states, may be the reason for the initial increase in the optical gap. Due to the increase in the Bi content, the formation of Bi-rich backbone clusters in the network is enhanced. Therefore, more addition of Bi causes an increase in the size of these clusters, which due to the lower thermal conductivity of the amorphous network, causes it to crystallize in the network. Their nucleation and growth with the increase in Bi content enhances the defect states associated with the inhomogeneous two-phase system or the constraint to the mixing of crystalline Bi-clusters and the amorphous network. The increase in these defect states may thus lead to the decrease in optical gap. The decrease in the optical gap may also be due to the formation of lower band gap phases such as Bi_2Se_3 and BiSe_2 . The quantity B^{-1} , which is determined from the slope of the Tauc plot of

$(\alpha h\nu)^{1/2}$ versus $(h\nu)$, can be taken as an approximate measure of the extent of band tailing into the band gap of the amorphous semiconductors. The values of B^{-1} obtained are listed in Table 1. As observed from Table 1, the values of B^{-1} decrease as Bi concentration increases from $x = 0$ to 6 and thereafter increases for $x = 8$. The rise and fall in the values of B^{-1} may be attributed to a decrease in the extent of localized tail states and due to the development of defect states by the addition of Bi.

Conclusion

Structural investigations of $\text{Sn}_{10}\text{Sb}_{20-x}\text{Bi}_x\text{Se}_{70}$ ($0 \leq x \leq 8$) system using X-ray diffractograms and SEM techniques have been reported. It is found that the compositions with $x = 0$ and 2 are amorphous in nature but the samples with $x = 4, 6$, and 8 show sharp peaks. These peaks are due to the formation of Bi_2Se_3 and BiSe_2 phases confirmed from JCPDS files. The presence of these phases is also confirmed from SEM and DSC studies. Various parameters related to optical properties have been calculated for all the compositions. Change is observed in the values of n and k with the change in Bi content and it is due to the change in stoichiometry and internal strain of the glassy alloy with the change in Bi content. The optical band gap initially increases at lower Bi concentration and then decreases sharply for higher Bi content. The change is explained on the basis of network modification with the increase in Bi content.

References

1. Frenichs R (1950) *Phys Rev* 78:643
2. Frenichs R (1953) *J Opt Soc Am* 43:1153
3. Hilton AR (1970) *J Non-Cryst Solids* 2:28
4. Cardinal T, Richardson KA, Shim H, Schulte A, Beatty R, Le Foulgoc K, Meneghini C, Viens JF, Villeneuve A (1999) *J Non-Cryst Solids* 353:256
5. Efimov OM, Glebov LB, Richardson KA, Van Stryland E, Cardinal T, Park SH, Couzi M, Bruneel JL (2001) *Opt Mater* 17:379
6. Stronski AV, Vlcek M, Sklenar A, Shepeljavi PE, Kostyukovich SA, Wagner T (2000) *J Non-Cryst Solids* 973:266
7. Salimnia A, Villeneuve A, Galstyan TV, Larochelle S, Richardson K (1999) *J Lightwave Technol* 17:837
8. Morgan WE, Van Wazer JR (1973) *J Phys Chem* 77:964
9. Moulder JF, Sticker WF, Sobol PE, Bomben KE (1992) *Handbook of x-ray photoelectron spectroscopy*. Perkin-Elmer, Eden Prairie, MN
10. Kastner M (1973) *Phys Rev B* 7:5237
11. Tanaka K (1989) *Phys Rev B* 39:1270
12. Guman SJ et al (1989) *J Non-Cryst Solids* 833:227
13. Kumar P, Kumar J, Ahmad M, Thangaraj R (2008) *Appl Phys A* 90:469
14. El-Korashy A, El-Kabany N, El-Zahed H (2005) *Physica B* 365:55
15. Kastner M, Adler D, Fritzsche H (1976) *Phys Rev Lett* 37:1504
16. Tohge N, Yamamoto Y, Minami T, Tanaka M (1979) *Appl Phys Lett* 34:640
17. Lucovsky G, Nemanich R, Galeener FL (1977) In: Spear W (ed) *International conference on amorphous and liquid semiconductors*, CICL, University of Edinburg, Edinburg, p 130
18. Kerr JA (2000) *CRC handbook of chemistry and physics*, 81st edn. CRC Press, Boca Raton, FL
19. Pauling L (1967) *The nature of the chemical bond*. Oxford & IBH, Delhi
20. Swanepoel R (1983) *J Phys E Sci Instrum* 16:1214
21. Tauc J (1979) *Amorphous and liquid semiconductors*. Plenum, New York

